The contribution of XANES spectroscopy to tribology[1]

M. Nicholls, M.N. Najman, Z. Zhang, M. Kasrai, P.R. Norton, and P.U.P.A. Gilbert

Abstract: X-ray absorption near edge structure spectroscopy (XANES) analysis has been routinely used to study the complex chemical interactions between additives in engine oil and metallic surfaces during high-temperature and pressure reciprocating wear conditions. XANES analysis provides detailed chemical and structural information on the resultant antiwear and tribo films formed on metallic surfaces. The following review will illustrate how XANES analysis on the macro scale can provide the information required to elucidate complex film formation mechanisms, then describes the use of emerging XANES spectromicroscopy to such systems, and concludes by showing the complementary nature of the macro and micro scale spatially resolved XANES analysis; Professor Bancroft has utilized the combination of these to stay at the forefront of XANES research in the field of tribology and in spectroscopy science in general.

Key words: tribology, XANES, X-ray absorption near edge structure spectroscopy, metals, thiophosphates, spectromicroscopy, tribochemistry.

Résumé : L'analyse des spectres de la structure fine d'absorption des rayons X près du seuil (« XANES ») a été utilisée d'une façon routinière pour l'étude des interactions chimiques complexes entre les additifs des huiles à moteur et les surfaces métalliques, dans des conditions de températures et de pressions élevées qui provoquent des usures réciproques. Les analyses de type « XANES » permettent d'obtenir des informations chimiques et structurales détaillées sur les films anti usure/tribo résultants qui se forment sur les surfaces métalliques. La revue qui est présentée ici permettra d'illustrer comment les analyses de type « XANES » à l'échelle macro peuvent fournir l'information requise pour élucider les mécanismes complexes de formation de films et ensuite décrire l'utilisation de la spectromicroscopie de type « XANES » qui se développe à l'étude de tels systèmes avant de conclure en mettant en évidence la nature complémentaire des études de type « XANES » résolues dans l'espace aux échelles micro et macro; la combinaison qui a été utilisée par le professeur Bancroft pour lui permettre de demeurer à la tête des méthodes de type « XANES » dans le champ de la tribologie et dans le domaine de la spectroscopie en général.

Mots-clés : tribologie; « XANES », spectroscopie de la structure fine d'absorption des rayons X près du seuil, métaux, thiophosphates, spectromicroscopie, tribochimie.

[Traduit par la Rédaction]

Introduction

In 1966 the term tribology was coined by the newly formed Committee on Tribology of the British House of Commons. Tribology can be defined as the science and technology of interacting surfaces in relative motion and of related subjects and practices (1). It encompasses a wide variety of topics and is a truly interdisciplinary field of study. One of the core disciplines of tribology is chemistry, termed tribochemistry, and presents a most challenging approach to understanding the history of a rubbing contact, the dynamic nature of the contact, the protective film formation process, and attrition during wear. In one combination or another, a wide range of chemical and analytical techniques have been used to understand the tribochemistry of a system. These include X-ray photoelectron spectroscopy (XPS) (2–7), Auger electron spectroscopy (AES) (8–12), energy dispersive X-ray (EDX) analysis (13–15), IR spectroscopy (16–21), and transmission electron microscopy (TEM) (8, 22).

It is the formulation and study of engine oils and how they decompose in solution and between rubbing contacts that comprises a vast majority of the associated literature on how additives work. Until 1986, X-ray absorption spectroscopy (XAS) was an unexplored technique in the investigation of tribological contacts (23). X-Ray absorption spectroscopy probes the transition of electrons from core states and is particularly useful for low-Z elements (such as C, N, P, O, and S, common elements found in additive molecules). Spectra allow for the collection of a comprehensive

Received 25 April 2007. Accepted 18 July 2007. Published on the NRC Research Press Web site at canjchem.nrc.ca on 29 August 2007.

M.A. Nicholls.[2] Dofasco Inc., Research and Development, Hamilton, ON L8N 3J5, Canada.
M.N. Najman. Lubrizol Corporation, Wickliffe, OH, USA.
Z. Zhang. Milacron Inc, Cincinnati, OH, USA.
M. Kasrai and P.R. Norton. The University of Western Ontario, Department of Chemistry, London, ON, Canada.
P.U.P.A. Gilbert.[3] Department of Physics, University of Wisconsin-Madison, Madison, WI, USA.

[1]This article is part of a Special Issue dedicated to Professor G. Michael Bancroft.
[2]Corresponding author (e-mail: mark_nicholls@dofasco.ca).
[3]Previously publishing as Gelsomina De Stasio.

 doi:10.1139/V07-093

set of data that provide details on geometry, oxidation state, and quantum numbers of the absorbing atom. Chemical changes, which result from the additives breaking down or interacting during rubbing, are observed as changes in the absorption structures in the recorded spectra (24–26).

Advancements in the area of nanotechnology have demanded an improvement in the spatial resolution of many surface analytical techniques, and XAS is not impervious to these pressures. In fact, XAS has welcomed these advancements and has made some very significant strides towards providing spatially resolved chemical speciation to <100 nanometer spatial resolution (27–30). The first use of spatially resolved XAS, termed X-ray photoelectron emission spectromicroscopy (X-PEEM), was published on the reaction films formed from organo-molybdenum compounds in a tribo-contact in 1997 (31). As the technique evolved and improved, many other groups exploited it in the study of tribology (32–36).

The use of XAS, or more specifically X-ray absorption near edge structure (XANES) spectroscopy, and subsequently X-PEEM began to be embraced by the tribology community after a chance meeting at an Ontario Center for Materials Research (OCMR) meeting in 1990. At that meeting G.M. Bancroft and M. Kasrai from the University of Western Ontario (UWO) introduced XANES to a major lubricant manufacturer, Imperial Oil. At that time, Dr. Kim Fyfe from Imperial Oil was looking for a technique that could easily characterize the chemical form of phosphorus and sulfur. After a short explanation and introduction to the approach, which G.M. Bancroft and M. Kasrai were exploiting at that time to investigate the intricate and detailed chemistry of coals and bitumus materials, an almost 10-year relationship began between the UWO and Imperial Oil. This chance meeting has led to the co-authorship of 15 publications by the three researchers and allowed for the crossing of paths with two other very prominent researchers at Chevron, Dr. Elaine Yamaguchi and Ray Ryason in 1994. The collaboration with Chevron continues today with over 15 joint publications. This has established the UWO group as the leading world experts in the study of tribochemistry by XANES spectroscopy, with a total of 55 publications with associates over the last 15 years. At the root of these publications is the ability of XANES spectroscopy to elucidate the lubrication properties of antiwear additives, determine mechanisms by which certain oil additives perform, but also be able to explain their behavior at a fundamental chemical level.

Examples of the type of work performed over the last 15 years will be briefly discussed in this paper to demonstrate the usefulness of XANES in the study of tribochemistry. The first section will highlight the information XANES spectroscopy has provided about the macrochemistry of the tribofilms generated from dialkyl-dithiophosphates (and derivatives thereof) on steel surfaces, and how this information can be used to explain the growth and wear processes experienced in the rubbing contact. The second section will illustrate the more advanced, spatially resolved, microchemical characterization done with X-PEEM. The section will describe how this approach helps to identify the location and chemical speciation of an antiwear film formed on a high silicon content (~18%) aluminum–silicon alloy, which is beneficial to understanding the applicability of such an alloy in a combustion engine. The final section will demonstrate the value of combining XANES and X-PEEM results to comprehensively evaluate both the tribochemical make-up as well as topographical features of lubricious films generated from ashless phosphorus- and sulfur-containing additives. This introduction presents the wealth of information that XANES spectroscopy has provided to the tribology community, and clearly demonstrates how the group at the UWO has maintained their dominance in the field by exploiting its emerging capabilities.

Experimental

Sample preparation and film formation

The steel samples were manufactured from 52100 steel into square specimens 10 mm × 10 mm × 4 mm or 19 mm diameter discs. The composition of 52100 steel is ~1% C, 1.3%–1.6% Cr, and the remainder primarily Fe. The steel samples were polished with 3 μm diamond paste. The aluminum 390 (A390) material was wire electrode discharge machined to create 10 mm × 10 mm × 4 mm samples. The composition range of A390 is ~4%–5% Cu, 16%–18% Si, with small percentages of Mg, Fe, Zn, and Ti. The A390 samples were polished with 0.3 μm alumina and finished with 0.05 μm silica suspension. The reciprocating cylinders were manufactured from 52100 steel, 6 mm in diameter and 6 mm in length. The steel sample and pins were austenitized and quenched. Their hardness was >60 Rockwell C. The pins were used as is.

The antiwear films were formed in a reciprocating Plint wear tester (37) under boundary lubrication conditions with a cylinder-on-flat test geometry establishing a line contact. The test conditions consisted of rubbing times that varied between 10 s and 10 h, at varying temperatures 60–100 °C, with a frequency of 25 Hz, load between 60–220 N, and a 7 mm stroke length. Chemical structures of the additives used in this study are shown in Fig. 1. A ZDDP commercial concentrate was obtained from Imperial Oil Limited, Canada. The concentrate is a mixture of neutral and basic forms, consisting of 85% secondary (C-4) and 15% primary (C-8) alkyls. The concentrate was diluted using MCT-10 base oil to 1.2 mass% resulting in a phosphorus content of ~0.1% by weight. MCT-10 base oil is a mineral oil with a sulfur content of 0.12 mass%. Two different ashless thiophosphate additives were used. The first additive used was an ashless triaryl monothiophosphate and is referred to as MTP. The second additive used was an ashless dialkyldithiophosphate and is referred to as DTP. The lubricant formulation was achieved by dissolving the additive by weight in the low sulfur base stock. The concentrations used in this study were 0.5 wt% DTP and 1.5 wt% MTP, respectively. The antiwear films were stored as is with their oily protective layer. Before insertion into vacuum the samples were thoroughly rinsed in hexanes. The light hydrocarbon rinse has been found not to alter the antiwear film, which is very robust (38, 39). On the X-PEEM samples, a grid composed of indent marks was created using a Vickers hardness tester. This grid allowed for relocation of the same regions with the multiple techniques discussed below.

Fig. 1. Chemical structures of antiwear additives: zinc dialkyldithiophosphate (ZDDP), triaryl monothiophosphate (MTP), ashless dialkyldithiophosphate (DTP), and commercial additive Irgalube 349.

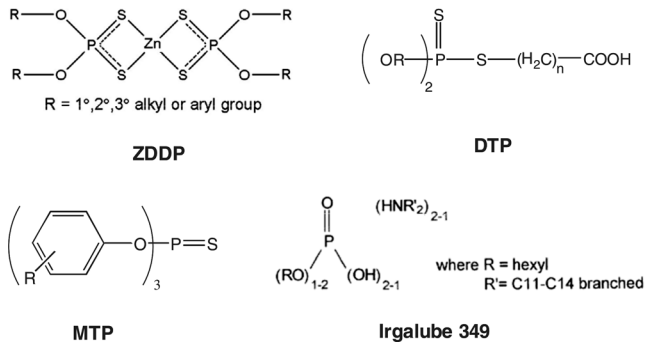

Surface imaging

Topographical imaging was performed using a Digital Instruments Nanoscope IIIa® atomic force microscope. Images were obtained in constant force mode to investigate the morphology and topography of the blank substrates, wear scars, and antiwear films after formation. A LEO-440 scanning electron microscope with a Quartz Xone Gresham light element detector was used to image the surfaces in field-emission and backscattering modes and to perform X-ray analysis.

XANES and X-PEEM analysis

X-ray absorption spectra provide detailed information about the local environment and oxidation state of elements in a film or on a surface. XANES analysis employs the use of soft X-rays making it a nondestructive technique. XANES spectroscopy was performed at the Canadian Synchrotron Radiation Facility at the 1 GeV Aladdin storage ring, University of Wisconsin, Madison. The data were obtained using the Grasshopper beamline, which has a resolution of ~0.1 eV, and the double crystal monochromator (DCM) beamline with a photon resolution of ~0.9 eV. Spectra were recorded using the total electron yield (TEY) and fluorescence yield (FY) detection modes (details of which can be found elsewhere (40)), and represent the information from a surface several square millimetres in area. The sampling depths of the TEY and FY at the P K-edge are 50 nm and >800 nm, respectively (41), and the sampling depths of the TEY and FY at the P L-edge are 5 and 60 nm, respectively (41). These techniques are ideally suited for measuring antiwear films such as these, which are on the order of 50–100 nm thick. At least two individual scans were recorded for each specimen and digitally combined. The spectra were normalized against I_o, and a linear background was subtracted.

X-ray photoelectron emission spectromicroscopy was performed using the SPHINX (42) microscope (ELMITEC GmbH), with an optimum spatial resolution of 10 nm (42), installed on the 6m-TGM (toroidal grating monochromator) beamline at the 1 GeV Aladdin storage ring, University of Wisconsin, Madison, optimized to give ~0.1 eV resolution at the phosphorus L-edge (for details see refs. 32, 43, and 44). Image intensity in X-PEEM is proportional to the TEY, and the surface sensitivity was limited by the escape depth of the secondary electrons at the phosphorus L-edge (3–5 nm) (41, 43). For the phosphorus L-edge region, a "stack" consisting of 301 images were taken over an energy range of 130–160 eV with an energy spacing of ~0.1 eV. A 100 μm field of view was chosen for the selected areas with a resolution of ~200 nm per pixel. Typical areas examined were <10 μm^2. The images were combined to produce a three-dimensional data set or spectromicroscopy movie (29) that was analysed to extract detailed chemical information about the tribofilm using aXis2000 software (28, 45). The data analysis procedure and the obstacles overcome have been described elsewhere (28, 29, 45, 46). Briefly, the aXis2000 software enables the selection of a single pixel, or regions of interest of several pixels in size, from which XANES spectra are extracted. The resulting spectra are averaged over all the pixels contained in the region of interest. Thus, some spectra are the average of a few pixels (usually with poor signal-to-noise) or several tens or hundreds of pixels.

Contributing evidence to the usefulness of XANES in the study of tribolochemistry

As examples of the value of XANES to the study of tribology, this first section will highlight the information that XANES spectroscopy has provided about the macrochemistry of the tribofilms generated from dialkyldithiophosphates. The second section will illustrate the more advanced, spatially resolved, microchemical characterization done with X-PEEM. The final section will demonstrate the value of combining XANES and X-PEEM results to comprehensively evaluate both the tribochemical make-up as well as topographical features of lubricious films generated from ashless phosphorus- and sulfur-containing additives.

A. Study of the tribochemistry of ZDDP and DTP using XANES

XANES measurements have been found to be ideally suited to the chemical studies of these films. First, most of the important elements in these films (e.g., P and S) have suitable absorption peaks (e.g., P and S L- and K-edges) in the soft-X-ray energy region. Some of these provide better chemical resolution than other analytical techniques. Second, TEY and FY detection modes allow for nondestructive study of the chemical nature of the surface, the near surface region, and the bulk of the film.

Zinc dialkyldithiophosphate (ZDDP) has been used for many years as the most common and the best antiwear (AW) additive for engine lubricant formulations. ZDDP is contained in fully formulated combustion engine oils at less than 0.1 wt% phosphorus content. Current environmental regulations are driving research to develop other AW additives that contain less phosphorus, since this element poisons catalytic converters leading to increased NO_x exhaust emissions. Despite the wide use of ZDDP, the formation, composition, and function of sacrificial wear films produced from its decomposition products are only partially understood. However, it is now widely accepted that ZDDP tribofilms consist mainly of phosphates with some sulfides (47), and the average thickness of the films is less than 100 nm (39).

Sarin et al. (48) showed that ashless thiophosphates gave comparable antiwear and antioxidant properties to those of

Fig. 2. Phosphorus L-edge XANES (in TEY mode) spectra of model compounds and tribofilms generated from 1 wt% ZDDP (left) and DTP (right) for different rubbing times.

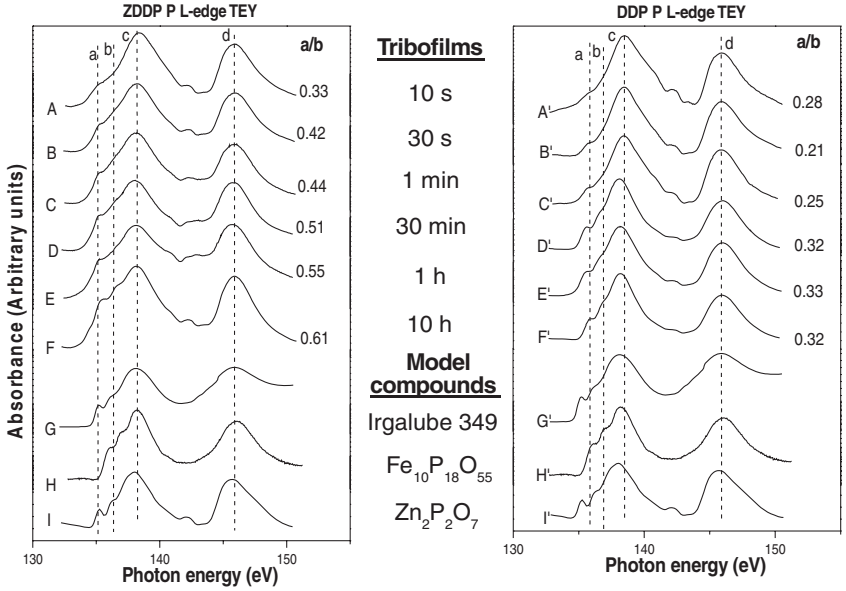

ZDDP in bench tests. In contrast to the ZDDP film chemistry, XANES analysis showed that DTP gave short-chain polyphosphates throughout the film, and the sulphide formed was largely FeS (49). It was assumed that the cation in the phosphate glass was Fe^{2+}. This section will describe the use of XANES to the study of ZDDP and DTP tribofilm products and how the detailed chemical and structural data can be interpreted to theorize the decomposition and film formation mechanisms.

Results and discussion

Phosphorus characterization

Phosphorus L-edge XANES spectra of tribofilms generated from ZDDP and DTP at different rubbing times and model compounds are shown in Fig. 2. These spectra are characteristic of polyphosphate glasses observed in all of our previous studies of both ZDDP and DTP films (49–55). Comparing the ZDDP spectra in Fig. 2 (left), it can be seen that the peak positions in spectra A to F of the tribofilms generated at different rubbing times are highly similar to the positions for the model compound, zinc polyphosphate ($Zn_2P_2O_7$). In particular, the position of peak a in the tribofilms is much closer to peak a for Zn polyphosphate than for Fe polyphosphate or a phosphate ester, Irgalube 349. This indicates that the major cation in the surface of these films is Zn^{2+} rather than Fe^{2+} or Fe^{3+} and is consistent with our previous findings that films formed for long rubbing times have long-chain Zn polyphosphates at the surface and shorter-chain Zn polyphosphates (with some Fe) in their bulk (50–55). X-ray photoelectron spectroscopy (XPS) also showed that there is no Fe the in surface of the films (56). The peak located at ~142 eV is due to carbon contamination of the beamline optics and is a 2nd order carbon peak (32, 46). The intensity of peaks a or b relative to peak c has been used to indicate the phosphate chain length; an a/c of about 0.3 is representative of a short-chain polyphosphate, and an a/c of about 0.6 indicates a long-chain polyphosphate (57). The FY spectra of ZDDP films provide chemical information about the bulk and indicate that the chain length is shorter (a/c of <0.4) for the long rubbing time films, an a/c of ~0.6 from the surface sensitive TEY measurement as observed previously (e.g., see Figs. 2E, 2F). These spectra show the bi-layer nature of the ZDDP films having short-chain polyphosphates in the bulk and long-chain polyphosphates at the surface.

However, the present results on ZDDP antiwear films show, for the first time, that the polyphosphate chain length at the surface of these films increases with rubbing time. For spectrum A from the 10 s film, the ratio of intensity of peak a/c is 0.33, indicating a short-chain zinc polyphosphate. With increasing rubbing time, the a/c ratio of the spectra (A to F) increases. Thus, for the 10 h film (spectrum F), the a/c ratio is 0.61. Because the Zn/P ratio of 1:2 in ZDDP is much smaller than the Zn/P ratio in a short-chain polyphosphate (e.g., 1:1 in $Zn_2P_2O_7$), the initial formation of a short-chain polyphosphate indicates that substantial Fe must be present in these shorter rubbing time films. The availability of Fe (or Fe oxides) from the steel surface decreases as the film becomes thicker, and the chain length increases with relatively more Zn and less Fe in the surface of the films. Unfortunately, the position of peak a is not sensitive to the differences in the relative proportion of Fe and Zn in these films and therefore no direct evidence supports this.

The spectra of the DTP films (Fig. 2, right) are qualitatively similar to the ZDDP spectra — they are all characteristic of polyphosphates. However, there are two obvious differences. First, the position of peak a in all spectra aligns very well with peak a for $FePO_4$ rather than $Zn_2P_2O_7$, suggesting that, as expected, Fe is the predominant cation in these films (the shoulder in the ZDDP spectra), which appears just before peak a, is due to the presence of a small amount of unreacted ZDDP (50, 51). Second, the ratio a/c in all spectra is close to 0.3, indicating that all films contain short-chain polyphosphates as was found earlier by Najman

Fig. 3. Oxygen K-edge XANES spectra of model compounds and tribofilms generated from 1 wt% ZDDP (left) and DTP (right) for different rubbing times.

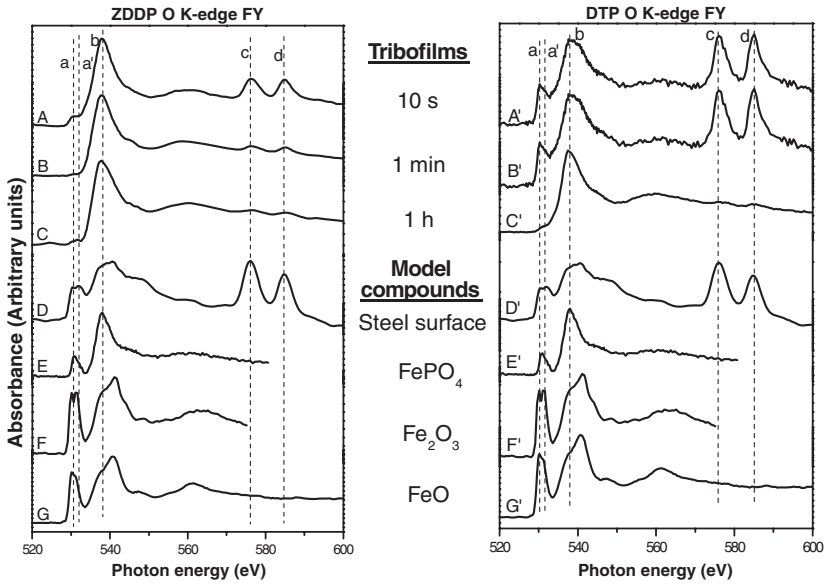

(55). It is not easy to rationalize why DTP gives short-chain polyphosphate, especially for the thick films, when the availability of cations for DTP has to be less than that for ZDDP. However, careful examination of spectra shows that position of peak c in spectra D′ to F′ (30 min to 10 h films) shifts slightly (~0.5 eV) to lower energy corresponding to zinc polyphosphate or Irgalube 349 spectrum G′. This suggests that in the absence of Fe as a cation, contaminant zinc and (or) an alkyl group are balancing the charge in these films. The alkyl group may originate from incomplete decomposition of DTP. Our recent studies on phosphate esters indicate that the P L-edge spectra of some of the organic phosphates are similar to those of metal phosphates (55).

Oxygen characterization and the role of Fe in the films

Oxygen K-edge FY XANES spectra of tribofilms generated from ZDDP and DTP at different rubbing times and model compounds are shown in the left and right panels of Fig. 3, respectively. The TEY spectra for all of these samples (not shown) are qualitatively similar. Spectra A (A′) to C (C′) are produced from tribofilms rubbed for 10 s, 1 min, and 1 h, respectively. Peaks c and d in some of these spectra originate from chromium L-edge XANES from a concentration of the 1% Cr in the 52100 steel surface oxide. This may indicate that the probing depth is greater than 500 Å and large enough to detect the steel surface in these very thin films; however, there could also be Cr incorporated into these phosphate films as suggested by XPS broad scans (not shown). Peak a is very weak in the ZDDP spectra (A and B) showing a rather small amount of Fe in these films. In contrast, the spectra A′ and B′ from the DTP films show a very intense peak a without any noticeable a′. This certainly indicates that there is appreciable Fe phosphate in these films, although there is still a contribution to these spectra from the surface Fe oxide. However, after one hour of rubbing (spectrum C′), peak a is very weak (although stronger than in the comparable ZDDP spectrum C), indicating rather little Fe is in the films. If Fe is the only cation (or even the predominant cation due to some Zn incorporation) in these phosphate films, the intensity of peak a should be much larger in spectrum C′. On the other hand, it was shown in Fig. 2 for 30 min to 10 h films, that contaminant zinc cations and alkyl groups may balance the charge for these phosphates. We cannot, at present, explain this apparent discrepancy.

Fe L-edge results for Fe characterization

The iron L-edge spectra of the films and model compounds taken with second-order synchrotron light (24) are shown in Fig. 4 for the ZDDP films (left) and DTP films (right). As for the oxygen K-edge spectra, the $FePO_4$ spectrum (D) is appreciably different from those of the oxides: peak a is very narrow and not split as with the other three Fe standards (spectra E, F, and G). For ZDDP films, the 10 s film (A) shows mostly Fe oxides. However for the thicker 1 min and 1 h ZDDP films (B and C), the spectra are very weak, showing that there is very little Fe in the surface of these films. For the very thin DTP films (A′ and B′) and thick film (C′) the spectra are very similar to the Fe oxide from the steel surface. This is not surprising. As was shown in Fig. 6 of reference (56), the DTP films were very inhomogeneous and are composed of small pads compared to the ZDDP films. Furthermore, scratch marks are quite apparent in these films and obviously the Fe signal may originate from the substrate, although a contribution may also be given by the small amount of iron phosphate that can exist in the film.

Sulfur characterization

Sulfur K-edge XANES spectra of tribofilms generated from ZDDP and DTP at different rubbing time and model compounds are shown in Fig. 5. The spectra of the ZDDP films (spectra A, B, and C) are highly similar to the ZnS spectrum (with peak c dominating), as reported in our previous studies (58, 59). This indicates that the main chemical state of sulfur in the tribofilms generated from ZDDP at all rubbing times is ZnS. However, for the 10 sec film (spec-

Fig. 4. Fe L-edge XANES spectra (recorded with second-order light) of model compounds and tribofilms generated from 1 wt% ZDDP (left) and DTP (right) for different rubbing times.

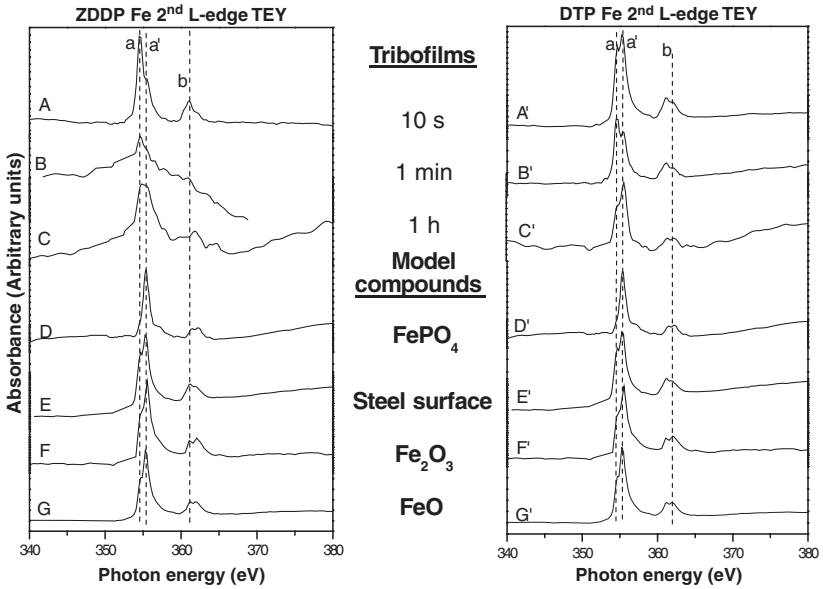

Fig. 5. Sulfur K-edge XANES spectra of model compounds and tribofilms generated from 1 wt% ZDDP and DTP for different rubbing times.

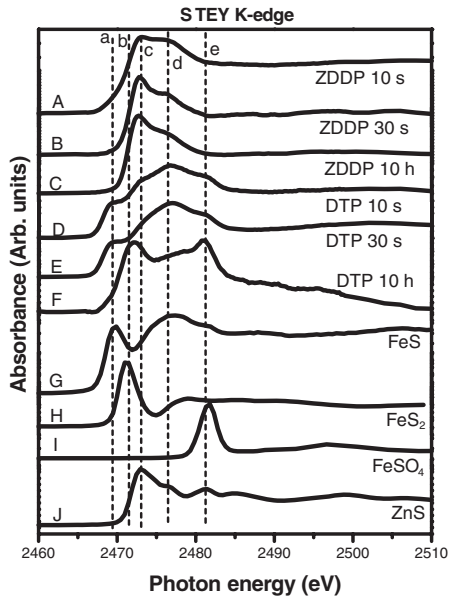

trum A) there are two shoulders, peaks a and d. These two shoulders correspond to the FeS spectrum (spectrum G). This result implies that there are two kinds of sulfides in the tribofilm generated from 10 sec rubbing. Zinc sulfide is the main chemical state of sulfur, but there is also some iron sulfide in the film. Because the concentration of iron sulfide is lower, there are only two shoulders in spectrum A, and this indicates that iron sulfide does exist in the tribofilm at the beginning of rubbing; and more importantly, Fe from the surface is immediately available for reaction with the sulfur and (or) phosphorus generated as the ZDDP decomposes. As rubbing continues, peak a disappears and the intensity of peak d decreases. This indicates that the amount of FeS in the film decreases relative to the amount of ZnS. In the thick films, there is probably only FeS right at the interface between the tribofilm and the steel surface. This is not unexpected from the principle of hard acids and soft bases as outlined by Martin and co-workers (60, 61). The soft base S^{2-} prefers to react with the borderline soft acid Zn^{2+} over the harder acid Fe^{2+} or Fe^{3+}. This principle can also be expressed by thermodynamic predictions. For example, consider the reactions,

[1] $$FeS + Zn^{2+} \rightarrow ZnS + Fe^{2+}$$

or

[2] $$FeS + ZnO \rightarrow FeO + ZnS$$

ΔG^0 is negative for these two reactions because of the very large negative ΔG_f^0 for ZnS (–201.3 kJ/mole) compared with FeS (–100.4 kJ/mole) (62). In the presence of a Zn species, FeS is expected to convert to ZnS. However, the majority of the zinc ends up in Zn polyphosphates rather than ZnS. The very large ΔH_f^0 values (ΔG_f^0 values are not available (62)) for the Zn phosphates (e.g., –2892 kJ/mole for $Zn_3(PO_4)_2$ and –4479 kJ/mole for $Zn_3P_4O_{13}$) indicate that the Zn phosphates are the thermodynamically stable zinc products in this complex system. For example, the ΔG value is –145 kJ for the following reaction,

[3] $$3ZnS + 2\ H_3PO_4 \rightarrow Zn_3(PO_4)_2 + 3H_2S$$

Indeed, the presence of Zn in the DTP films from a very minor zinc contamination shows that Zn phosphates are incredibly stable compounds. The XPS data shown elsewhere (56) support this discussion. In DTP films in the absence of Zn (or very small amount due to contamination), the sulfur proportion (~1%) is very low compared with that of ZDDP films (~8%).

For the DTP films, Najman (55) already reported that substantial FeS was present in these films after rubbing for greater than 5 min. The formation of FeS is much clearer in

the 10 s and 30 s films, as shown in Figs. 5D and 5E; indeed, FeS is the dominant sulfur species in these two spectra.[4] The presence of peak c in these spectra could be due to a small amount of ZnS from the contaminant Zn. The 10 h film shows the presence of sulfate (peak e) and some FeS and FeS_2, with perhaps a small amount of ZnS.

Sulfur K-edge XANES spectra of tribofilms generated from different concentrations of ZDDP were also investigated (not shown). The spectra of sulfur in the different concentration tribofilms are the same and align with zinc sulfide. This indicates that the concentration of ZDDP does not affect the formation of zinc sulfide in the tribofilm.

From the preceding discussion, it can be concluded that the tribofilm generated from ZDDP is a multilayer film. The mechanism of tribofilm formation for both ZDDP and DTP is given in more detail below.

A. ZDDP Mechanism

(Products entering solution are ignored.)
Stage 1. Physical and chemical adsorption.

[4] $Zn[(RO)_2PS_2]_2$ (solution) $\rightarrow Zn[(RO)_2PS_2]_2$ (ZDDP adsorbed)

Stage 2. Initial film formation (~10 nm) on the surface when cations are plentiful.

[5] $Zn(RO)_4P_2S_4 + O_2$ (in oil) + FeO $\rightarrow$ Zn/Fe phosphate (short-chain) + ZnS + FeS

Stage 3. Surface is covered with a thin film and Fe is not accessible from the substrate.

[6] $Zn(RO)_4P_2S_4 + O_2$ (in oil) $\rightarrow$ Zn phosphate (long-chain) + ZnS

In stage 2 based on ΔH_f^0 values, the proportion of FeS will be very small. In stage 3, Zn phosphate formation is preferred over ZnS formation.

Stage 4. Conversion of long-chain polyphosphate to short chain.

[7] Zn phosphate (long-chain) + $6H_2O \rightarrow$ Zn phosphate (short-chain) + $4H_3PO_4$

In stage 4, any water in the system can hydrolyze long-chain polyphosphates to short-chain (53, 63). As a result, the film becomes thicker, composed of short-chain Zn phosphate (with little Fe). We can think of a tri-layer film, with the top layer consisting of longer chain phosphates, a middle layer of predominantly short-chain phosphates, and an inorganic layer of ZnS and (or) FeS.

B. DTP Mechanism

(Products entering solution are ignored.)
Stage 1. Physical/chemical adsorption.

[8] $(RO)_2PSS\text{-}C_2H_4CO_2R$ (solution) $\rightarrow (RO)_2PSS\text{-}C_2H_4COOR$ (DTP adsorbed)

Stage 2. Initial film formation (~10 nm) on the surface when Fe are plentiful.

[9] $(RO)_2PSS\text{-}C_2H_4CO_2R + O_2$ (in oil) + FeO $\rightarrow$ Fe phosphate (short-chain) + FeS

Stage 3. Surface is covered with a thin film of Fe phosphate and no cation is accessible from the substrate.

[10] $(RO)_2PSS\text{-}C_2H_4CO_2R + O_2$ (in oil) + H_2O (in oil) $\rightarrow$ phosphate ester + alkyl sulphide

In stage 3, the alkyl sulphide will be dissolved in oil. However, it is difficult to see how the phosphate ester can remain on the surface.

Conclusions

The macro-scale XANES spectra yield much information about the film chemistry. The phosphorus L-edge spectra (along with the oxygen K-edge spectra and Fe L-edge spectra) have been used for the first time to give information on the role of Fe in the films. For ZDDP, a bi-layer phosphate film develops very quickly. Initially, the film is predominantly short-chain polyphosphate with Zn as the predominant cation, but the film develops to give predominantly long-chain Zn polyphosphate at the surface and a shorter chain polyphosphate with some Fe in the bulk. The average polyphosphate chain length increases with an increase in ZDDP concentration up to a certain point. For DTP, the polyphosphate film is of short-chain character throughout the test, with cations being Fe and alkyl groups. The proportion of alkyl groups is much higher on the surface. At this stage we cannot give a quantitative estimate of the proportion of Fe in the tribofilm. The Fe from the oxide and from solution must become available at the high local temperatures for the phosphate film formation, even for the relatively thick films. Some sulfur from the ZDDP reacts to form ZnS, but in addition the presence of FeS has been identified for the first time in the early films from both ZDDP and DTP.

This study demonstrates how XANES spectroscopy can provide detailed chemical information on complex heterogeneous tribofilms formed on steel. It goes further by illustrating how this information can be interpreted to elucidate complex film formation mechanism. A next step in understanding such complex systems would be able to spatially extract the same comprehensive information from discrete locations on a surface. Synchrotron spectromicroscopy has enabled the acquisition of chemical information on the submicron length scale (27, 29, 32, 44, 64) and opened up the ability to investigate, for the first time, the spatial distribution and chemical speciation of antiwear (AW) films.

[4] In the case of tribofilms, the formation of a pure compound is rarely observed. Typically, intermediate species are incorporated in the film as a result of incomplete chemical reactions. Thus, the use of the term dominant to indicate that the major sulfur component of the film, in this case, is FeS.

B. X-ray photoelectron emission spectroscopy of ZDDP films on Al–Si alloys

Not only are replacement additives for ZDDP being sought to reduce emissions, but automotive manufacturers are also envisioning weight savings by altering the design of the engine block to reduce fuel consumption and therefore also reduce emissions. Aluminum–silicon alloys with high silicon contents (>18%) are currently being investigated as cost effective replacements for cast iron components. The introduction of silicon improves the wear resistance of aluminium through the formation of separate hard phase silicon grains in the aluminum matrix. A long-standing question is the function of the silicon grains. It is generally thought, since very little research exists, that the grains, after honing and etching of the surface, act like riders that bear the load of the conforming surface (65–69). To date no suitable additive has been found which can effectively lubricate Al–Si alloys. It would be ideal if ZDDPs proved to be effective additives to reduce friction and wear of Al–Si alloys.

For the first time, the spatial localization,and chemical speciation of ZDDP AW films on high silicon content Al–Si alloys was performed using X-ray photoelectron emission spectromicroscopy (X-PEEM). The ability to spatially resolve features on a surface enables examination of the occurrence (or lack thereof) and location of ZDDP AW film formation under lubricated wear of a high-silicon content (~18%) Al–Si alloys.

Results and discussion

Fiducially placed indents were used to recognize and reanalyse specific areas of interest, using atomic force microscopy (AFM), X-PEEM, and secondary electron microscopy (SEM). These indents were made after the ZDDP AW films were formed on the Al–Si alloy. As was performed previously (70), SEM imaging and EDX elemental mapping were used to understand the heterogeneous nature of the alloy surface and was performed after X-PEEM analysis. A high-resolution SEM image is shown in Fig. 6. The diamond-shaped indents used to identify the regions of interest are clearly observed, as are the distinct grey features that have been identified by EDX as silicon grains (70). Light wisps and blotches are due to the difference in backscattering from the agglomeration of other elements such as iron, copper, and magnesium.

Once a particular silicon grain was pinpointed, the region was then examined by AFM. AFM imaging provides high-resolution topographic information and has been routinely used to observe the varying morphology of AW films (71–73). In this instance, AFM was used to investigate where (if any) ZDDP AW films formed. ZDDP antiwear films on steel have a heterogeneous topography composed of islands and valleys. The islands have been termed AW pads and are thought to act like a cushion preventing the two rubbing surfaces from coming into contact (44). Figure 7A is a mosaic of AFM images that show a large silicon grain running diagonally across the figure. The large "diamond-shaped" indents can also be observed at the top and bottom. In AFM images, objects with a higher elevation appear lighter. Careful examination of the silicon grain shows small, elevated islands, or ZDDP AW pads. The pads have an elongation that is in the direction of the rubbing experienced during the friction test. A 3D AFM image of the AW pads, boxed 1 in Fig. 7A, is shown in Fig. 7B. The padlike morphology can be clearly observed and is quite similar to those formed on steel under identical rubbing conditions (70). Again, the pads are thought to limit the contact between the two rubbing surfaces. Since AFM imaging provides 3D topographic information it is possible to extract useful height information about the surface. A cross-sectional profile along the line (marked 2) in Fig. 7A is shown in Fig. 7C. From this profile the height of the silicon grain can be measured to be ~100 nm; as well, the oscillations on the surface of the grain can be identified as the small AW pads.

Fig. 6. A secondary electron image (in backscattering mode) of the Al–Si surface. Vicker's indents can be identified in the image as well as the distinct silicon grains.

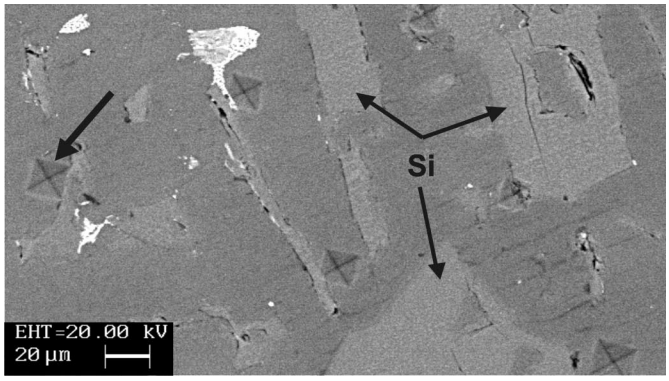

Advancements in X-ray photoelectron emission spectromicroscopy have made it possible to image surfaces similar to a secondary electron microscope. This gives the user the unique ability to distinguish small features on a surface (on a submicron scale), and then determine the chemical nature of the species present using X-ray absorption spectroscopy. This powerful combination of techniques has only become possible (at this resolution) in the last several years and has only been routinely used to analyse ZDDP AW films on steel recently (32, 44, 74). The imaging function of the X-PEEM was used to locate the same fiducial indents identified in with the AFM images. For comparative purposes, the AFM image is reintroduced in Fig. 8A with the X-PEEM image Fig. 8B (with the same orientation and scale as in the AFM image). The large indents can be observed, as well as the large AW pads (circled).

Using the X-PEEM analysis software, an image mask was generated to separate the ZDDP AW pads form all other features (details of the entire procedure can be found elsewhere (44)). Figure 9 shows the mask used to select only the large AW pads. The mask is used to extract and average the phosphorus L-edge spectra obtained from each pixel within the mask. The average spectrum using this procedure is labelled (D), shown in Fig. 10, and is compared with the model spectra from compounds with known oxidation state and elemental geometry around the phosphorus atom. Comparisons to unreacted ZDDP (A), a zinc polyphosphate glass (B), and a ZDDP AW film formed on steel, make interpretation of the film chemistry much easier. The spectrum from the unreacted ZDDP shows its characteristic triplet structure (51). The zinc polyphosphate has peaks a, b, and c that are shifted to higher energy from peaks 1, 2, and 3 of unreacted

Fig. 7. (A) A mosaic of AFM images showing a large silicon grain on the top of which patches of ZDDP antiwear film can be observed. The silicon grain runs diagonally through the image. (B) A 3D topographic image of the antiwear pads found within box 1. (C) A cross-sectional profile taken across 2.

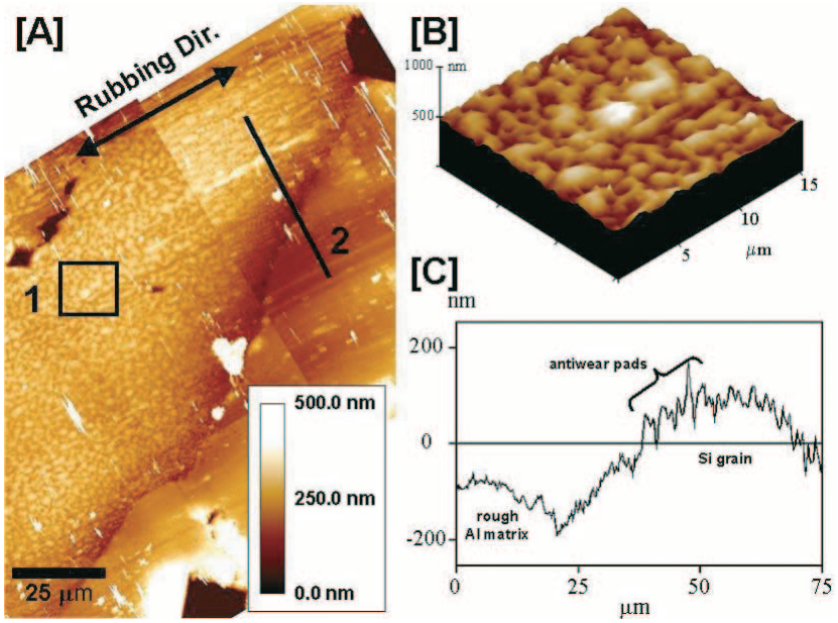

ZDDP. Peaks a and b are the 2p spin-orbit doublet, separated by 0.8 eV. They are assigned to the transitions of electrons from occupied $2p_{3/2}$ and $2p_{1/2}$ levels to unoccupied antibonding orbitals. Peak c is attributed to the transition of the 2p electrons to a p-like t_2* molecular orbital. As described previously, the ratio of the intensities of peaks a/b increase as the polyphosphate chain length increases (44, 57, 75). An *ideal* ZDDP AW film formed on 52100 steel (C) has a polyphosphate structure. Comparison of this spectrum (C) to that of the AW film formed on the Si grain (D) reveals that the AW film does have the characteristic polyphosphate structure as that formed by ZDDP on the steel surface.

In spectrum (D) the ratio is 0.65, and in spectrum (E) the ratio is 0.60. This indicates that the AW pads have a longer polyphosphate chain length than the off-pad areas (44, 57, 75). This would indicate that although the Al matrix is too soft to allow shear forces to reach a sufficient magnitude to decompose ZDDP, polyphosphates can form on the hard silicon grains and must transfer to the Al matrix. The shorter-chain polyphosphates as well as unreacted ZDDP were also found in regions off the silicon grains on the Al matrix (70). This is indicative of the sacrificial nature of ZDDP AW films as they form on steel. Spectrum (F) in Fig. 10 shows a small shoulder (labelled s) to the left of peak a that lines up well with unreacted ZDDP, indicating that ZDDP species are also located in the Al matrix.

These results show that X-PEEM is a powerful tool for the investigation of ZDDP AW action on Al–Si alloys. Topographic imaging has observed that the ZDDP antiwear films are formed of patches (termed antiwear pads), characterized as smooth plateaus between which valleys and *bare* surfaces have been found. X-PEEM analysis at the phosphorus L-edge identified polyphosphates in the ZDDP AW film. It was found that the antiwear pads were located on the hard silicon grains and were oriented in the direction of rubbing; furthermore, the AW pads had a slightly longer polyphosphate chain length than the lower (valley) and surrounding Al matrix regions. This indicates that not only does the ZDDP AW film formed on Al–Si alloys possess a similar polyphosphate structure to films formed on steel, but it also has the same sacrificial characteristic (whereby polyphosphate is transferred from the hard silicon grains to the softer Al matrix) that it does on steel surfaces.

Conclusions

The use of spatially resolved X-PEEM chemical analysis in combination with high-resolution topographic imaging have provided new insight into the location and structure of ZDDP AW films on Al–Si alloys. The combination of these techniques provides researchers with the unique ability to obtain useful data on the chemical nature and wear protection mechanisms of ZDDP, and thus provide insight into how new replacement additives need to function to perform as effectively as ZDDP.

The final section in this review will demonstrate the coupling of the powerful macro-scale XANES analysis (e.g., section A) with the unique X-PEEM ability of spatially resolving where the tribofilms have formed and determine their exact chemical make-up.

C. Investigating the microchemical properties of tribofilms generated from ashless thiophosphate additives

As shown above, XANES has focused primarily on the understanding of tribochemistry from reaction films generated from various types of ZDDPs. However, concerns over some of the potential environmental implications of using ZDDPs have created an increased interest in the understanding of how metal-free lubricant additives function (37, 48,

Fig. 8. The AFM image from Fig. 7 is re-introduced (A) for navigation, along with the (B) secondary electron X-PEEM image showing the silicon grain and antiwear pads. The large antiwear pads are circled in the AFM to aid in identification in the X-PEEM image.

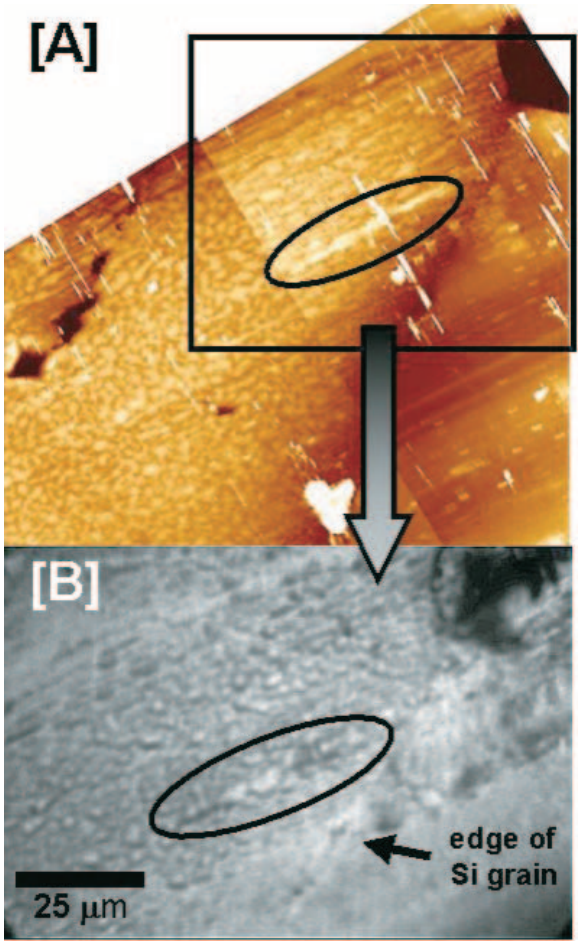

76). As a result, only recently has XANES been extended to that family of additives. Various types of phosphate esters as well as organosulfur compounds, such as sulfurized esters and dialkyldithiocarbamates, have been studied using XANES with much success (77, 78).

This section discusses the complementary use of macroscale XANES and X-PEEM to investigate the microchemical properties of lubricious films generated from ashless thiophosphate oil additives under boundary lubrication. During reciprocating sliding, noticeable differences were seen between an ashless dithiophosphate additive (DTP) and a monothiophosphate additive (MTP). Wear scar width measurements of the pin revealed that the DTP additive at a concentration of 0.5 wt% in sulfur-free base oil provided statistically better wear protection than the MTP additive at a concentration of 1.5 wt%. Preliminary tribochemical film analysis using X-ray photoelectron spectroscopy (XPS) and conventional XANES revealed slight differences in the phosphorus concentration at the near surface, while the polyphosphate structure, from a macrochemical perspective, was relatively the same between the two additives — both the MTP and DTP additives generated a short-chain

Fig. 9. A mask showing the selection of the larger ZDDP antiwear pads only. Spectra were extracted from only these regions to produce the spectrum shown in Fig. 10D.

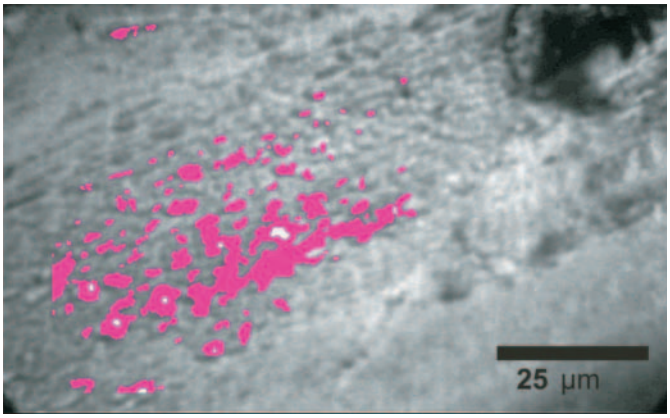

Fig. 10. (A) The XANES spectra for unreacted ZDDP, (B) a zinc polyphosphate, Zn4P6O16, and (C) ZDDP antiwear films formed on steel, (D) on silicon grain, (E) found between the antiwear pads on the silicon grain, and (F) on the aluminum matrix.

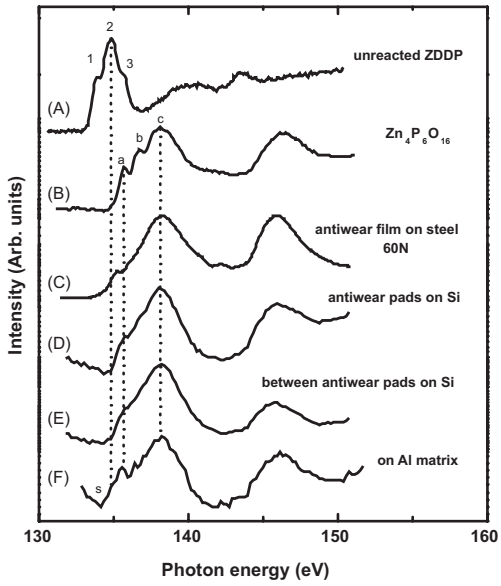

polyphosphate AW film (49, 79). Figure 11 displays the conventional macro XANES spectra (acquired from ~5mm^2 area) at the phosphorus L-edge for the tribochemical films generated from two ashless thiophosphate additives.

Results and discussion

The general topographical features of both MTP and DTP tribofilms were compared using both X-PEEM and AFM and are shown in Fig. 12. Based on the images, differences in the tribofilms are immediately apparent. For DTP, the 120 × 120 µm AFM image reveals a heterogeneous surface with elongated pads oriented in the sliding direction with widths between 2.5–5.0 µm as determined by X-PEEM. Conversely, the MTP tribofilm appears to be very homoge-

Fig. 11. Conventional P L-edge XANES spectra (from ~5 mm^2 area) of tribofilms generated from DTP and MTP in total electron yield (TEY) mode, compared with an iron polyphosphate model compound.

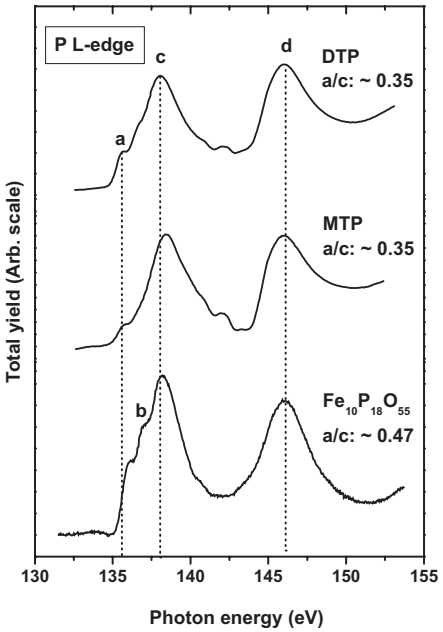

neous topographically, with thin elongated pads oriented in the sliding direction as well. Pad widths for the MTP tribofilm were estimated to be in the range of 1.5–2.0 μm.

Using X-PEEM analysis similar to that shown previously, the P L-edge region data showcase the properties of the AW films in a variety of ways. Figure 13b shows a "difference image" revealing the spatial distribution of polyphosphate from the DTP AW film excluding topographic information. The difference image technique subtracts two different spectral images along the phosphorus L-edge to show image contrast based on chemical and elemental properties. Figure 13a is a PEEM image of area of tribochemical film generated from the DTP additive taken at a photon energy of 137.2 eV. This on-peak image shows topography and chemistry combined. Figure 13b is a digital difference of two images, on-peak and off-peak, taken at 137.2 and 133.7 eV, respectively. Since the off-peak image contains only the topographic contribution, the difference image in Fig. 13b shows only the chemistry. Notice the presence of phosphorus on the surface of the tribofilm and its higher concentration (brighter pixels) where the pads are located. From the stack of difference images that can be created, one of the fascinating observations (not shown) is that the image intensity of the padlike structures begins to increase, eventually reaching a maximum intensity at the absorption edge.

As mentioned above, conventional XANES spectroscopy at the phosphorus L-edge samples an area on the order of several square millimetres, dimensions too large to provide any microchemical information (see Fig. 11 for example). On the SPHINX microscope,where the X-PEEM experiments were conducted with a field of view of 100 μm, in which each pixel represented an ~200 nm × 200 nm area, thereby enabling microchemical analyses. Figure 14 shows the X-PEEM image of an area where local XANES spectra

Fig. 12. Height mode atomic force microscope images and topographical PEEM image for the two AW films prepared: (a) DTP and (a) MTP.

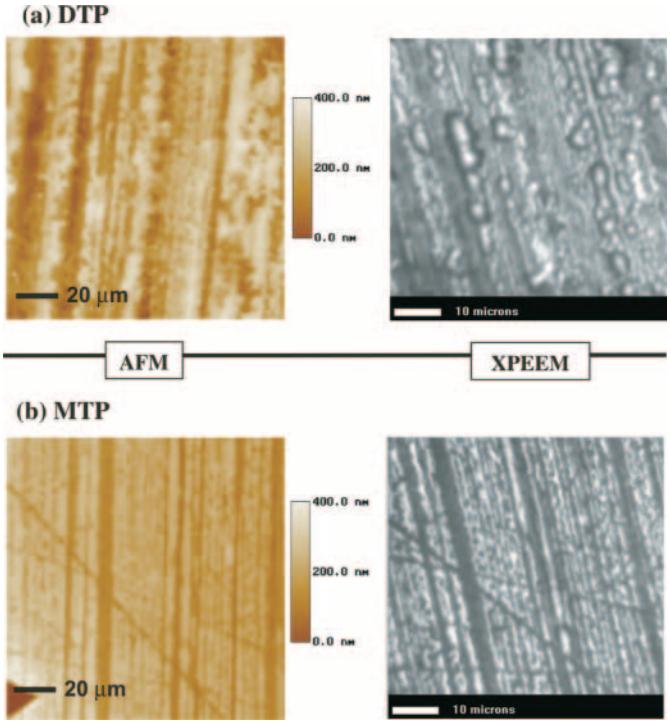

Fig. 13. (a) PEEM image of an area of tribochemical film generated from the DTP additive taken at a photon energy of 137.2 eV. This on-peak image shows topography and chemistry combined. (b) Digital difference of two images, on-peak and off-peak, taken at 137.2 and 133.7 eV, respectively. Since the off-peak image contains only the topographic contribution, the difference image in (b) shows only the chemistry.

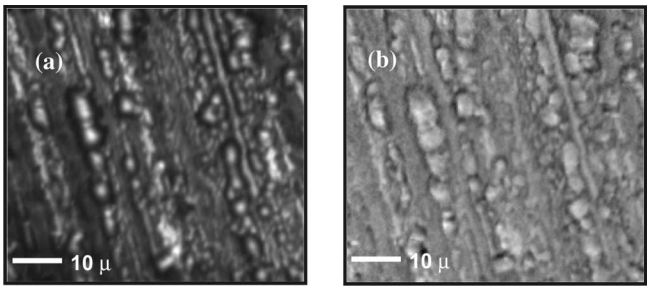

at the phosphorus L-edge were taken within the wear scar for the DTP AW film, and can be compared with Fig. 11 that displays the conventional macro XANES spectra. XANES spectra were extracted from several different areas within the respective X-PEEM image and are indicated by the labelled areas. Several regions were analysed to determine notable differences in polyphosphate chain length from pad to pad. Prior work from our group has shown that for phosphorus L-edge XANES spectra, the intensity of peaks a and b relative to peak c correlate very well to polyphosphate chain length i.e., a higher ratio of a/c suggests longer-chain polyphosphates (57) (also see the example in Section A).

Fig. 14. Detailed microchemical analysis of a region within the wear scar of AW film of DTP. (a) PEEM image with labeled areas indicating where local P L-edge XANES spectra were extracted. (b) Corresponding P L-edge XANES spectra.

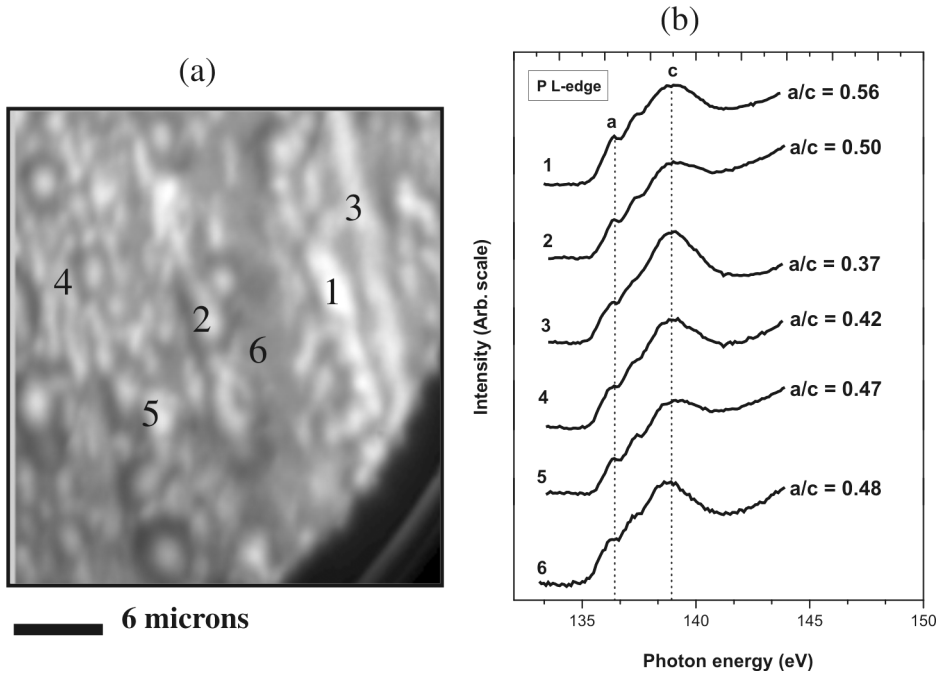

Fig. 15. Detailed microchemical analysis of a region within the wear scar for AW film of MTP. (a) PEEM image with labeled areas indicating where local P L-edge XANES spectra were extracted. (b) Corresponding P L-edge XANES spectra.

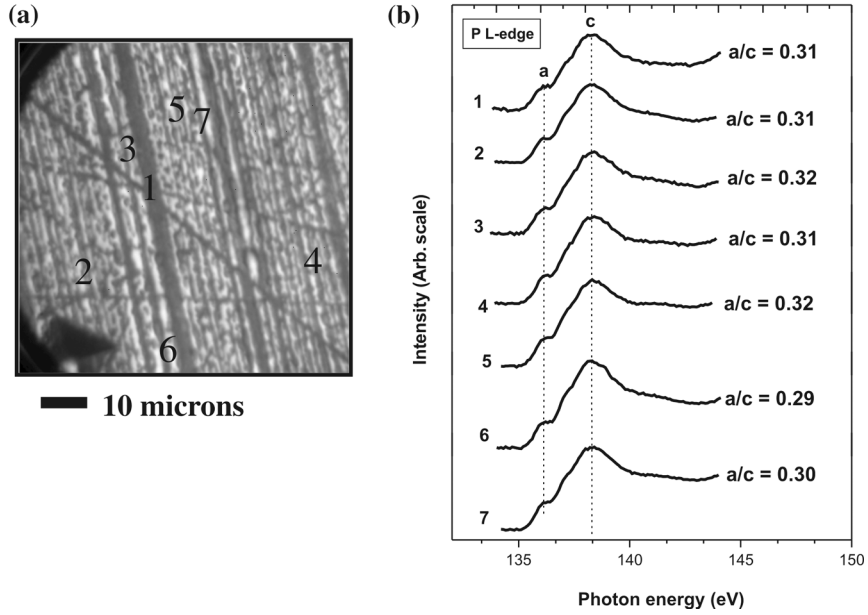

With this in mind, the a/c ratios of the different regions are shown beside the corresponding phosphorus L-edge spectra, 1–6, respectively. Looking at both the local XANES spectra and the corresponding ratios, it is clear that while the different regions do look similar to one another spectrally, there are variations in the microchemical properties of the DTP film, with local areas consisting of varying degrees of polyphosphate chain length.

Focusing on the microchemical properties of the MTP AW film, X-PEEM reveals differences when compared with DTP. The X-PEEM image of the MTP AW film in Fig. 15, along with the corresponding extracted spectra, clearly shows microchemical homogeneity throughout the analysed area of the film (again, these microchemical spectra can be compared with Fig. 11, which displays the conventional macro XANES spectra). Focusing on the a/c ratios, there is little or no change across individual pads. Several different areas were also investigated (not shown) with similar results, thus concluding that the AW pads that are developed during tribofilm formation are predominantly or almost completely

Fig. 16. Example of chemical mapping depicting polyphosphate chain length distribution within an area of AW film generated from DTP. (a) Topographical X-PEEM image displaying selected regions of interest. (b) Spectra 1 and 2 correspond to the raw P L-edge XANES spectra of regions 1 and 3 in (a). Spectra 3 and 4 correspond to residual P L-edge XANES spectra of regions 1 and 3 after a spline background was removed. (c) Derived quantitative chemical maps of the two components used. Spectra 3 and 4 were used as the components to generate the maps. (d) Color-coded composite map displaying polyphosphate chain length distribution. Areas of longer chain polyphosphates are colored in magenta, while green depicts areas of shorter chain polyphosphates.

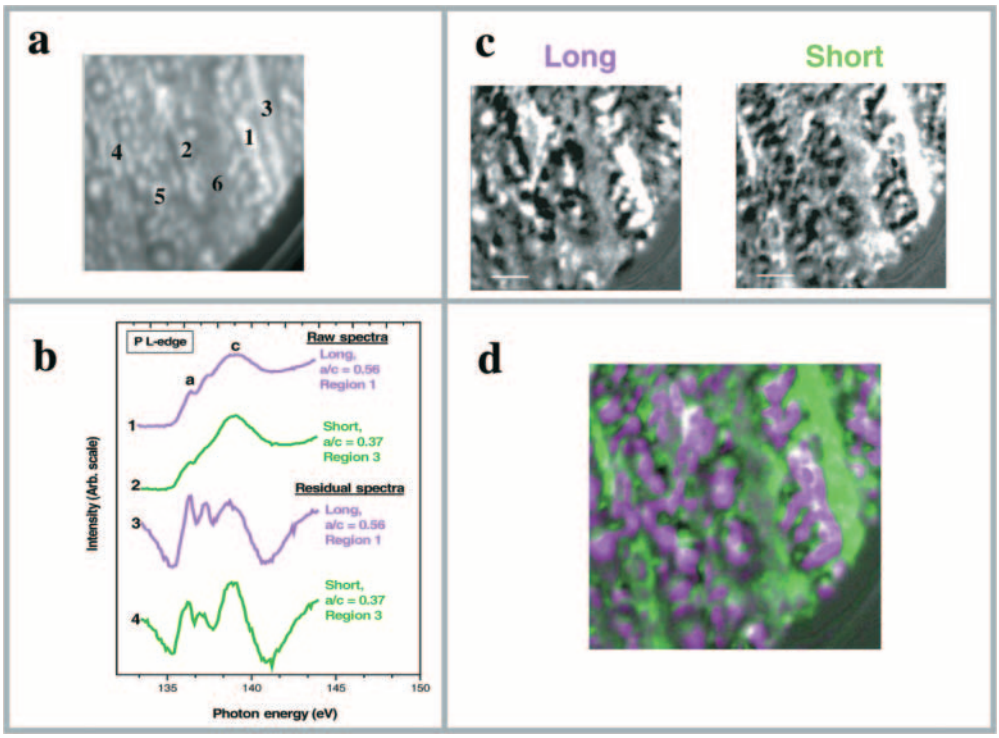

short-chain polyphosphates. Recalling results obtained from conventional XANES, surprisingly, the polyphosphate chain length between the two AW films was similar (Fig. 11).

The ability to extract local XANES spectra at the submicron level clearly demonstrates the power of X-PEEM and how useful it is in the field of tribology. X-PEEM was able to discriminate between areas of different polyphosphate chain lengths within an AW film for the DTP additive on the basis of intensity ratio of peaks a to c in the phosphorus L-edge. Another advantage of X-PEEM is that the intensity of the peaks observed can also be used as individual components to obtain a chemical distribution map, of varying polyphosphate chain length, from the set of images collected. There are several references in the literature describing the use of quantitative analytical techniques to extract these types of maps from a wide range of materials including polymers and proteins (29, 30, 64). Briefly, a linear regression analysis was applied pixel-by-pixel to the acquired image sequence to derive the component maps. This allows for full spectral variation to be used in deriving the maps. Since the tribofilms studied are not comprised of one pure component but rather a mixture, no quantitative reference standards exist thus making the analysis semiquantitative (80).

Looking at a spatial distribution map of polyphosphate chain length for the DTP AW film in Fig. 16, different regions within the AW film are clearly differentiated visually. To generate the colour-coded map in Fig. 16d, a spline background was removed from the raw phosphorus L-edge XANES spectra, and the spectra depicting areas of both longer- and shorter-chain polyphosphates were used as individual components for the map. The individual components are shown in Fig. 16c. The more intense bright areas reveal concentrated areas of shorter- and longer-chain polyphosphate for each component, respectively. The phosphorus L-edge spectromicroscopy reveals that there are areas of long-chain polyphosphates that are segregated from areas of shorter-chain polyphosphates, and upon closer inspection there are regions where both types coexist (black in Fig. 16d). White regions are where there were difficulties fitting to either spectra (typically because of lack of signal). The consistency of the colour-coded map was evaluated spectroscopically in 19 different areas (data not shown). Here the a/c peak intensity values were extracted from the phosphorus L-edge XANES spectra and tested against the map to determine its validity. It was found that the microchemistry along the various selected areas of interest was in good agreement with the map.

Conclusions

In general, this in-depth analysis of the tribochemical films generated from ashless thiophosphate oil additives clearly demonstrates the powerful capabilities of the X-PEEM technique, a clear extension of the macro XANES information that was originally acquired at the phosphorus L-edge. With X-PEEM, high quality submicron XANES spec-

tra can be obtained with phenomenally high energy and spatial resolution. Coupling the power of this technique with other topographical imaging techniques such as AFM has created an entirely new and exciting way to evaluate tribochemical structure–performance relationships for lubricant additives.

Concluding remarks

Undoubtedly XANES analysis has provided tribologists with a wealth of knowledge over the last 20 years. This brief review illustrates how XANES can probe common elements in additives and provide unique information. The three examples described above take the science from its beginning: macro-scale XANES has provided detailed chemical and structural information on antiwear and tribo films on metallic surfaces with enough illumination that complex and theoretically sound reaction mechanisms could be proposed. The review then reveals the more recent advancements in the field of XANES spectromicroscopy, in which complex surfaces can be imaged with submicron resolution, which enables the user to extract detailed XANES spectra from small discrete features. The last example summarizes the previously described macro- and micro-scale XANES approaches by coupling the methods to provide a complementary and compelling combination to spatially resolve where the tribofilms have formed and to determine their exact chemical make-up.

With this we dedicate our sincere thanks to G.M. Bancroft, a great friend and mentor, for guiding us through our research and ushering us into the forefront of XANES research through its use in tribochemistry at metallic surfaces.

Acknowledgements

The authors would like to personally thank A.P. Hitchcock for his help with aXis2000 and useful discussions about the analysis of the X-PEEM data. The authors would also like to thank K. Tan, A. Jurgensen, and the staff of the Synchrotron Radiation Centre (SRC), University of Wisconsin, Madison, for their technical support. M.A.N. would personally like to thank Heather Bloomfield and Ross Davidson of Surface Science Western, The University of Western Ontario, for acquisition and discussion about the SEM results. We are grateful to the National Science Foundation for supporting the SRC under Award # DMR-0537588. Financial support was provided by General Motors of Canada Ltd. and the Natural Sciences and Engineering Research Council of Canada (NSERC).

References

1. P. Jost. Tribol. Lubr. Technol. **3**, 24 (2006).
2. J.M. Martin, C. Grossiord, K. Varlot, B. Vacher, and J. Igarashi. Tribol. Lett. **8**, 193 (2000).
3. J.A. McGeehan, E.S. Yamaguchi, and J.Q. Adams. SAE Tech. Paper Ser. 852133, 1 (1985).
4. J.C. Bell, K.M. Delargy, and A.M. Seeney. Proc. Leeds–Lyon Symp. Tribol. **21**, 387 (1992).
5. K.J. Bird and G.D. Galvin. Wear, **37**, 143 (1976).
6. H. Spedding and R.C. Watkins. Tribol. Int. **99**, 9 (1982).
7. K. Varlot, J.M. Martin, C. Grossiord, R. Vargiolu, B. Vacher, and K. Inoue. Tribol. Lett. **6**, 181 (1999).
8. C. Grossiord, J.M. Martin, T. Le Mogne, and T. Palermo. Tribol. Lett. **6**, 171 (1999).
9. T.P. Debies and W.G. Johnston. Lubr. Eng. **23**, 289 (1980).
10. S. Jahanmir. J. Tribol. **109**, 577 (1987).
11. M. Kano, Y. Mabuchi, T. Ishikawa, A. Sano, and T. Wakizono. Lubr. Sci. **11**, 365 (1999).
12. P. Kapsa, J.M. Martin, C. Blanc, and J.M. Georges. J. Lubr. Technol. **103**, 486 (1981).
13. J.M. Martin, J.L. Mansot, I. Berbezier, and H. Dexpert. Wear, **93**, 117 (1984).
14. A.F. Alliston-Grenier, J.A. Greenwood, and A. Cameron. IMechE Conf. **178**, 565 (1987).
15. F.T. Barcroft, R.J. Bird, J.F. Hutton, and D. Park. Wear, **77**, 355 (1982).
16. M. Aktary, M.T. McDermott, and J. Torkelson. Wear, **247**, 172 (2001).
17. A. Molina. Lubr. Eng. **30**, 479 (1987).
18. P.A. Willermet, L.R. Mahoney, and C.M. Bishop. Lubr. Eng. **23**, 217 (1979).
19. P.A. Willermet, R.O. Carter III, and E.N. Boulos. Tribol. Int. **25**, 371 (1992).
20. F.M. Piras, A. Rossi, and N.D. Spencer. Tribol. Lett. **15**, 181 (2003).
21. F.G. Rounds. Lubr. Eng. **21**, 91 (1978).
22. J.M. Martin. Tribol. Lett. **6**, 1 (1999).
23. J.M. Martin, M. Belin, J.L. Mansot, H. Dexpert, and P. Lagarde. Lubr. Eng. **29**, 523 (1986).
24. J. Stohr. NEXAFS Spectroscopy. Vol. 25. Springer-Verlag, NY. 1992.
25. D.C. Koningsberger and R. Prins. X-ray absorption: Principles, applications, techniques of EXAFS, SEXAFS, and XANES. Vol 92. John Wiley and Sons, Toronto. 1988.
26. D. Norman. J. Phys. C: Solid State Phys. **19**, 3273 (1986).
27. C. Morin, H. Ikeura-Sekiguchi, T. Tyliszczak, R. Cornelius, J.L. Brash, A.P. Hitchcock, A. Scholl, F. Nolting, G. Appel, D.A. Winesett, K. Kaznacheyev, and H. Ade. J. Electron. Spectrosc. Relat. Phenom. **121**, 203 (2001).
28. L.M. Croll, J.F. Britten, C. Morin, A.P. Hitchcock, and H.D. H. Stoever. J. Synchrotron. Rad. **10**, 265 (2003).
29. C. Jacobsen, S. Wirick, G. Flynn, and C. Zimba. J. Microsc. **197**, 173 (2000).
30. X. Zhang, R. Balhorn, J. Mazrimas, and J. Kirz. J. Struct. Biol. **116**, 335 (1996).
31. H. Ade, A.P. Smith, H. Zhang, G.R. Zhuang, J. Kirz, E.G. Rightor, and A. Hitchcock. J. Electron. Spectrosc. Relat. Phenom. **84**, 53 (1997).
32. M.A. Nicholls, G.M. Bancroft, P.R. Norton, M. Kasrai, G. De Stasio, B.H. Frazer, and L.M. Wiese. Tribol. Lett. **17**, 245 (2004).
33. D.S. Grierson, A.V. Sumant, A.R. Konicek, M. Abrecht, J. Birrell, O. Auciello, J.A. Carlisle, T.W. Scharf, M.T. Dugger, P.U.P.A. Gilbert, and R.W. Carpick. J. Vac. Sci. Technol. A. In press. (2007).
34. A.V. Sumant, P.U.P.A. Gilbert, D.S. Grierson, A.R. Konicek, M. Abrecht, J.E. Butler, T. Feygelson, S.S. Rotter, and R.W. Carpick. Diamond Relat. Mater. In press. (2007).
35. J. Stohr and S. Anders. IBM J. Res. Develop. **44**, 535 (2000).
36. K. Masenelli-Varlot, M. Kasrai, G.M. Bancroft, G. De Stasio, B. Gilbert, E.S. Yamaguchi, and P.R. Ryason. Tribol. Lett. **14**, 157 (2003).
37. U. Wallfahrer and L. Bowen. Lubr. Eng. **53**, 23 (1997).

38. G.M. Bancroft, M. Kasrai, M. Fuller, Z. Yin, K. Fyfe, and K.H. Tan. Tribol. Lett. **3**, 47 (1997).
39. M.L. Suominen Fuller, L.R. Fernandez, G.R. Massoumi, W.N. Lennard, and M. Kasrai. Tribol. Lett. **8**, 187 (2000).
40. M. Kasrai, Z. Yin, G.M. Bancroft, and K. Tan. J. Vac. Sci. Technol. A, **11**, 2694 (1993).
41. M. Kasrai, W.N. Lennard, R.W. Brunner, G.M. Bancroft, J.A. Bardwell, and K.H. Tan. Appl. Surf. Sci. **99**, 303 (1996).
42. B.H. Frazer, M. Girasole, L.M. Wiese, T. Franz, and G. De Stasio. Ultramicroscopy, **99**, 87 (2003).
43. B.H. Frazer, B. Gilbert, B.R. Sonderegger, and G. De Stasio. Surf. Sci. **537**, 161 (2003).
44. M.A. Nicholls, P.R. Norton, G.M. Bancroft, M. Kasrai, T. Do, B.H. Frazer, and G. De Stasio. Tribol. Lett. **17**, 205 (2004).
45. A.P. Hitchcock, P. Hitchcock, C. Jacobsen, C. Zimba, B. Loo, E. Rotenberg, J. Denlinger, and R. Kneedler. aXis2000 [computer program]. Available from http://unicorn.mcmaster.ca/aXis2000.html. 1997.
46. M.A. Nicholls, T. Do, P.R. Norton, G.M. Bancroft, M. Kasrai, T.W. Capehart, Y.-T. Cheng, and T. Perry. Tribol. Lett. **15**, 241 (2003).
47. Z. Yin, M. Kasrai, G.M. Bancroft, K.F. Laycock, and K.H. Tan. Tribol. Int. **26**, 383 (1993).
48. R. Sarin, A.K. Gupta, D.K. Tuli, A.S. Verma, M.M. Rai, and A.K. Bhatnagar. Tribol. Int. **26**, 389 (1993).
49. M.N. Najman, M. Kasrai, and G.M. Bancroft. Tribol. Lett. **17**, 217 (2004).
50. Z. Yin, M. Kasrai, M. Fuller, G.M. Bancroft, K. Fyfe, M.L. Colaianni, and K.H. Tan. Wear, **202**, 192 (1997).
51. Z. Yin, M. Kasrai, M. Fuller, G.M. Bancroft, K. Fyfe, and K.H. Tan. Wear, **202**, 172 (1997).
52. M. Fuller, Z. Yin, M. Kasrai, G.M. Bancroft, E.S. Yamaguchi, P.R. Ryason, P.A. Willermet, and K.H. Tan. Tribol. Int. **30**, 305 (1997).
53. M.L. Suominen Fuller, M. Kasrai, G.M. Bancroft, K. Fyfe, and K.H. Tan. Tribol. Int. **31**, 627 (1998).
54. M.L. Suominen Fuller, M. Kasrai, and G.M. Bancroft. Chemical applications of synchrotron radiation. Vol 12B. World Scientific, NJ. 2002. p. 1091.
55. M.N. Najman. Ph.D. thesis. Chemical interactions of metal-free oil additives with 52100 steel. Department of Chemistry. The Universtiy of Western Ontario, London, Ont., Canada, 2003.
56. Z. Zhang, E. Yamaguchi, M. Kasrai, and G.M. Bancroft. Tribol. Lett. **19**, 211 (2005).
57. Z. Yin, M. Kasrai, G.M. Bancroft, K.H. Tan, and X. Feng. Phys. Rev. B, **51**, 742 (1995).
58. Z. Zhang, M. Kasrai, G.M. Bancroft, and E.S. Yamaguchi. Tribol. Lett. **15**, 377 (2003).
59. E.S. Yamaguchi, Z. Zhang, M. Kasrai, and G.M. Bancroft. Tribol. Lett. **15**, 385 (2003).
60. J.M. Martin, C. Grossiord, T. Le Mogne, S. Bec, and A. Tonck. Tribol. Int. **34**, 523 (2001).
61. C. Minfray, J.M. Martin, C. Esnouf, T. Le Mogne, R. Kersting, and B. Hagenhoff. Thin Solid Films, **447/448**, 272 (2004).
62. D.D. Wagman, W.H. Evans, V.B. Parker, R.H. Schumm, I. Halow, S.M. Bailey, K.L. Churney, and R.L. Nuttall. Journal of physical and chemical reference data. Vol 11. The American Chemical Society and the American Institute of Physics for the National Bureau of Standards, Washington, DC. 1982.
63. D.E.C. Corbridge. Structural chemistry of phosphorus. Elsevier, NY. 1974.
64. I.N. Koprinarov, A.P. Hitchcock, C.T. McCrory, and R.F. Childs. J. Phys. Chem. B, **106**, 5358 (2002).
65. M. Kawamura and K. Fujita. Wear, **89**, 99 (1983).
66. T. Konishi, E.E. Klaus, and J.L. Duda. Tribol. Trans. **39**, 811 (1996).
67. Y. Wan, L.L. Cao, and Q.J. Xue. Tribol. Int. **30**, 767 (1997).
68. M. Fuller, M. Kasrai, J.S. Sheasby, G.M. Bancroft, K. Fyfe, and K.H. Tan. Tribol. Lett. **1**, 367 (1995).
69. M.A. Nicholls, P.R. Norton, G.M. Bancroft, and M. Kasrai. Wear, **257**, 311 (2004).
70. M.A. Nicholls, P.R. Norton, G.M. Bancorft, M. Kasrai, G. De Stasio, K.S.-I. Nicholls, and L.M. Wiese. Tribol. Lett. **18**, 261 (2005).
71. A.J. Pidduck and G.C. Smith. Wear, **212**, 254 (1997).
72. O.L. Warren, J.F. Graham, P.R. Norton, J.E. Houston, and T.A. Michalske. Tribol. Lett. **4**, 189 (1998).
73. S. Bec, A. Tonck, J.M. Georges, R.C. Coy, J.C. Bell, and G. Roper. Proc. R. Soc. London, Ser. A, **455**, 4181 (1999).
74. G.W. Canning, M.L. Fuller, G.M. Bancroft, M. Kasrai, J.N. Cutler, G. De Stasio, and B. Gilbert. Tribol. Lett. **6**, 159 (1999).
75. M. Kasrai, M. Fuller, M. Scaini, Z. Yin, R.W. Brunner, G.M. Bancroft, M.E. Fleet, K. Fyfe, and K.H. Tan. Lubricants and lubrication: Lubrication at the frontier. Vol 30. Elsevier Science B.V., Amsterdam. The Netherlands. 1995. p. 659.
76. K.K. Swami, S. Prakesh, P.K. Mondal, K.C. Dohhen, R. Sarin, D.K. Tuli, and A.K. Bhatnagar. Lubr. Sci. **14**, 385 (2002).
77. M.N. Najman, M. Kasrai, G.M. Bancroft, and A. Miller. Tribol. Lett. **13**, 209 (2002).
78. M.N. Najman, M. Kasrai, and G.M. Bancroft. Tribol. Lett. **14**, 225 (2003).
79. M.N. Najman, M. Kasrai, G.M. Bancroft, B.H. Frazer, and G. De Stasio. Tribol. Lett. **17**, 811 (2004).
80. A.P. Hitchcock, I. Koprinarov, K. Pecher, and E.M. Kneedler. Manuscript in preparation.